Jurnal Polimesin
Department of Mechanical Engineering
State Polytechnic of Lhokseumawe
http://e-jurnal.pnl.ac.id/polimesin
e-ISSN : 2549-1999 No. : 2 Month : April
p-ISSN : 1693-5462 Volume : 24 Year : 2026

Processing dates: received on 2026-2-20, reviewed on 2026-03-01, accepted on 2026-03-11 and online availability on 2026-04-25

Lower-temperature sintering and optimization ratio of SiO_2-TiO_2-B_2O_3-ZnO glass ceramic coatings for energy efficient tile

Faisal Habib*, Mahmuddin, Muhammad Imam Arif
Department of Mechanical Engineering, Universitas Muslim Indonesia, Makassar 90232, Indonesia
*Corresponding author: faizal.habib@umi.ac.id

Abstract

Conventional ceramic tile glazes typically require firing temperatures above 1180°C, leading to high energy consumption and production costs. Despite extensive studies on composition and crystallization, integrated optimization of oxide balance, crystallization kinetics, and energy efficiency at reduced temperatures remains limited. This study aims to develop and optimize SiO_2–TiO_2–B_2O_3–ZnO glass-ceramic coatings through a combined experimental and data-driven approach to achieve enhanced mechanical performance at lower sintering temperatures. A series of compositions were formulated using locally sourced raw materials and sintered at 1080–1160°C. The crystallization behavior was first characterized using Differential Scanning Calorimetry (DSC) and fitted with the Johnson–Mehl–Avrami–Kolmogorov (JMAK) kinetic model. Phase evolution and microstructure were examined through X-Ray Diffraction (XRD) and Scanning Electron Microscopy (SEM). Mechanical and optical performance were evaluated via Vickers microhardness testing, gloss measurement, and bulk density analysis. Multivariate regression and energy-performance correlation analysis were conducted using MATLAB. The results demonstrate that increasing TiO_2 content promotes heterogeneous nucleation, lowering crystallization peak temperature from 785°C to 725°C and increasing enthalpy release from 48 to 64 J/g. The Avrami exponent (n = 1.75–1.95) indicates three-dimensional crystal growth with mixed nucleation mechanisms. Vickers hardness improved from 515 HV to 670 HV with increasing TiO_2 concentration, while gloss moderately decreased due to enhanced crystalline fraction. The optimal composition (55 mol% SiO_2, 8 mol% TiO_2, 2 mol% B_2O_3, 2 mol% ZnO) achieved 648 HV, 63 GU, and a 12% reduction in firing energy, demonstrating the feasibility of energy-efficient coating design.

Keywords:
Glass-ceramic coating, silica–titania–boron oxide, low-temperature sintering, computational modeling, microhardness.

1 Introduction

The advancement of glass ceramic glazes for floor and wall tile applications has become an important focus in mechanical and materials engineering due to the increasing demand for high-performance and energy efficient surface coatings. In ceramic tiles, the glaze layer governs not only aesthetic characteristics such as gloss and color uniformity but also functional properties including hardness, wear resistance, and long-term durability [1][2]. Unlike conventional amorphous glazes, glass-ceramic coatings consist of fine crystalline phases uniformly dispersed within a residual glassy matrix. This hybrid microstructure enhances microhardness, abrasion resistance, and structural stability, making such systems particularly suitable for high-traffic and industrial applications [3][4].

The chemical composition of glass-ceramic coatings plays a decisive role in determining crystallization kinetics, phase evolution, and surface performance [5][6]. In the classical SiO_2–TiO_2–B_2O_3 ternary system, silica (SiO_2) acts as the primary network former, titania (TiO_2) functions as a nucleating agent promoting controlled crystallization, and boron oxide (B_2O_3) serves as a flux that reduces melt viscosity and facilitates sintering at lower temperatures [7]. Achieving an optimal balance among these oxides is essential. Increased TiO_2 concentration generally enhances nucleation density and surface mechanical properties, whereas excessive B_2O_3 suppresses crystallinity and reduces hardness despite improving surface gloss and melt fluidity [8][9]. The compositional interplay between these oxides directly influences the resulting microstructure and mechanical optical trade-off.

A comprehensive understanding of crystallization kinetics is therefore critical for controlling phase transformation during firing. The Johnson-Mehl-Avrami-Kolmogorov (JMAK) model remains widely applied for interpreting Differential Scanning Calorimetry (DSC) data and evaluating nucleation mechanisms, crystal growth dimensionality, and apparent activation energy [10]. Computational fitting of Avrami parameters using MATLAB or similar numerical platforms enables quantitative prediction of transformation behavior, thereby reducing experimental iterations and improving formulation efficiency [11]. Such modeling approaches are increasingly relevant for data-driven materials design.

Boron oxide exhibits a dual functional role in glass-ceramic systems. At moderate concentrations, B_2O_3 lowers the glass transition temperature and promotes densification, contributing to reduced firing temperatures and improved energy efficiency**,** an important consideration in industrial ceramic processing. However, excessive B_2O_3 may inhibit crystal growth and diminish surface mechanical properties [12]. Consequently, optimizing the SiO_2-TiO_2-B_2O_3 ratio constitutes a multivariable design problem requiring controlled experimentation and computational support to balance hardness, gloss retention, and thermal efficiency [13].

Microstructural refinement has been consistently correlated with enhanced mechanical properties in glass-ceramic coatings. Finer and uniformly distributed crystalline phases improve hardness and toughness, whereas coarse or aggregated grains reduce surface uniformity and optical quality [14]. Characterization techniques such as X-Ray Diffraction (XRD), Scanning Electron Microscopy (SEM), and microhardness testing remain indispensable for establishing the relationship between phase composition, morphology, and performance [15].

In parallel, sustainability considerations have become central in modern ceramic manufacturing. Controlled nucleation and compositional optimization enable crystallization at temperatures 60-100°C lower than conventional firing regimes, significantly reducing kiln energy consumption while maintaining functional performance [16]. Low-temperature and fast-firing processes, combined with computational optimization strategies, are increasingly adopted to improve energy efficiency and reduce carbon emissions in tile production [17].

In this study, the term “low-temperature sintering” refers to firing temperatures between 1080–1120°C, which are approximately 60–100°C lower than conventional industrial glaze firing temperatures typically exceeding 1180°C.

Methodologically, the integration of experimental characterization with computational modeling including Avrami kinetic analysis, multivariate regression, and response surface optimization has gained prominence in contemporary ceramic research. MATLAB-based regression and kinetic fitting approaches have demonstrated correlation coefficients exceeding $R^2 = 0.9$, confirming their predictive reliability in compositional optimization studies [18]. However, despite these advances, several limitations persist in the current body of literature.

First, only a limited number of studies have successfully combined oxide composition optimization, crystallization kinetics modeling, and energy consumption analysis within a unified experimental computational framework. Second, the utilization of locally available raw minerals, such as feldspathic fluxes and limestone deposits in Indonesia, remains insufficiently explored despite their economic and sustainability advantages. Third, although the Avrami kinetic model is widely employed, its application to multiphase glaze systems with non-ideal crystallization behavior still requires further refinement to address phase competition and microstructural heterogeneity [19][2].

In response to these gaps, the present study revisits and extends the SiO_2-TiO_2-B_2O_3 system by incorporating a minor ZnO modifier and integrating low-temperature sintering with MATLAB-assisted kinetic and regression modeling. The objective is to establish a quantitative relationship between oxide composition, crystallization behavior, microstructure, and mechanical performance while simultaneously evaluating energy implications under reduced firing temperatures. By employing locally sourced raw materials and a data-driven optimization framework, this work aims to provide a sustainable and reproducible approach for energy-efficient tile manufacturing in Indonesia [17][20].

The primary contribution of this research lies in the systematic integration of experimental synthesis, crystallization kinetics analysis, and multivariate predictive modeling to optimize glass-ceramic coatings under lower-temperature sintering conditions. The inclusion of ZnO as a minor modifier and the application of computational optimization tools provide an enhanced methodological framework for developing high-performance, energy-efficient ceramic coatings suitable for industrial implementation.

2 Research method

2.1 Raw materials and formulation

The experimental work employed locally sourced raw materials commonly available within Indonesian ceramic industries, including kaolin, feldspathic flux, dolomite, limestone, zinc oxide (ZnO), alumina (Al_2O_3), silica sand (SiO_2), colemanite ($Ca_2B_6O_{11}\cdot 5H_2O$) as the boron source, and titania (TiO_2). These materials were selected for their purity, cost-effectiveness, and compatibility with industrial glaze formulations.

Five representative compositions (A1–A5) were designed within the SiO_2–TiO_2–B_2O_3–ZnO system, while maintaining a constant total flux content (CaO + MgO + Na_2O + K_2O = 33 mol%). The main variable parameters were the molar ratios of SiO_2, TiO_2, and B_2O_3, whereas ZnO was fixed at 2 mol% as a minor fluxing modifier to enhance surface densification.

Each mixture was formulated based on the molar percentages listed in Table 1 and verified by X-Ray Fluorescence (XRF) analysis in Table 2. This compositional design ensured systematic variation suitable for regression and kinetic modeling.

Table 1. Chemical composition of raw materials in molar percentages

Sample	SiO_2	TiO_2	B_2O_3	CaO	MgO	Al_2O_3	Na_2O	K_2O
A1	60	2	3	15	5	7	4	4
A2	58	4	3	15	5	7	4	4
A3	57	6	2	15	5	7	4	4
A4	55	8	2	15	5	7	4	4
A5	53	10	1	15	5	7	4	4

Table 2. XRF of raw materials (wt%)

Element	Kaolin	Feldspar	Dolomite	Limestone
SiO_2	48.3	66.5	1.2	3.5
Al_2O_3	36.2	17.0	0.5	0.3
CaO	0.4	0.9	31.8	52.4
MgO	0.2	0.4	18.5	1.0
Fe_2O_3	1.5	0.8	0.3	0.2

All compositions were prepared in duplicate batches to ensure consistency of raw material blending and to minimize compositional deviation prior to coating application.

2.2 Powder preparation and coating process

The raw powders were oven-dried, sieved to less than 75 µm, and dispersed in deionized water to form a stable slurry. To achieve homogeneous particle distribution, each formulation was milled in a planetary ball mill for 6 h using zirconia media with a ball-to-powder ratio of 3:1. A dispersant (sodium hexametaphosphate, 0.2 wt%) was added to prevent particle agglomeration during milling.

The prepared slurry was sprayed onto pre-cleaned stoneware tile substrates (50×50×8 mm) using a pneumatic spray gun to ensure a uniform coating thickness of approximately 0.3 mm. The coated specimens were pre-dried at 100°C for 2 h to remove residual moisture and minimize the risk of thermal shock during sintering.

Sintering was carried out in an electric muffle furnace under three different firing regimes: 1080°C, 1120°C, and 1160°C. Each regime employed a heating rate of 10°C/min and a holding period of 30 min at the peak temperature. An additional reheating step near 940–980°C for 20 min was applied to promote controlled crystallization, enhance nucleation, and reduce internal stresses.

The firing and heat-treatment conditions are summarized in Table 3, and the corresponding temperature–time profiles are illustrated in Fig. 1.

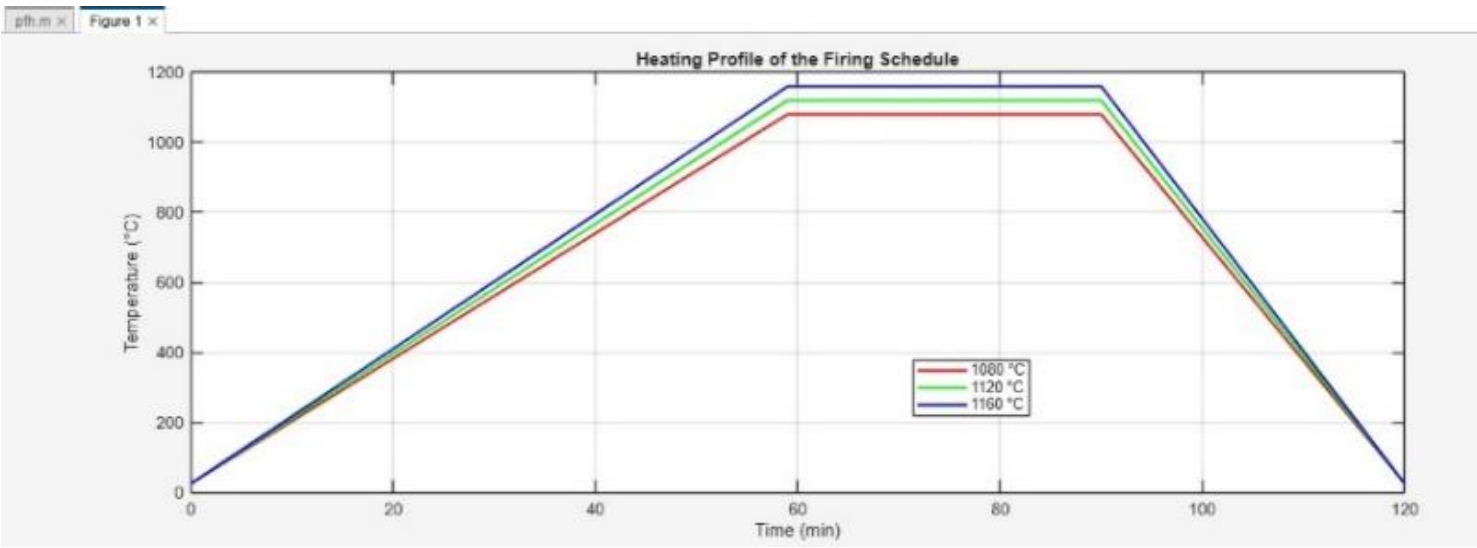

Fig. 1. Heating profile of the firing schedule.

Table 3. Firing and heat treatment schedule

Temp (°C)	Heating rate (°C/min)	Hold time (min)	Crystallization step (°C/min)
1080	10	30	940 / 20
1120	10	30	960 / 20
1160	10	30	980 / 20

Coating thickness variation was monitored using a digital thickness gauge, and the average thickness deviation was maintained within ±5% to ensure comparable firing and densification conditions among samples.

2.3 Characterization techniques

A combination of microstructural, thermal, optical, and mechanical analyses was conducted to evaluate coating performance and verify crystallization behavior.

XRD: phase identification was performed using Cu-Kα radiation (λ = 1.5406 Å), scanned from 10°–80° 2θ at 2°/min. The crystalline phases were identified with reference to ICDD standards to detect diopside, anorthite, or Zn-bearing silicates formed during firing.

DSC: non-isothermal DSC analysis was conducted at 10 °C/min from room temperature to 900°C to determine the crystallization onset (T_x), peak temperature (T_p), and enthalpy (ΔH) of each sample. The resulting thermograms shown in Fig. 2 were analyzed using the Avrami kinetic approach to determine the activation energy and growth parameters, as listed in Table 4 and Table 5.

SEM: surface morphology and grain distribution were observed at 10,000× magnification. Micrographs were used to correlate crystalline size and density with hardness and gloss, as discussed in Section 3.2.

Microhardness test: Vickers hardness (HV) was measured using a 50 g load and 10 s dwell time on polished cross-sections as shown in Table 6. The mean of five indentations for each sample varied with oxide composition and firing temperature.

Gloss measurement: surface reflectivity was measured with a digital glossmeter at an incidence angle of 60°, expressed in Gloss Units (GU). The data provided insight into the optical trade-off between crystal formation and surface smoothness.

Bulk density: determined by the Archimedes method using distilled water immersion, confirming densification trends consistent with SEM results.

To ensure measurement reliability, microhardness and gloss tests were performed at five different locations on each sample surface. The reported values represent the arithmetic mean of the measurements. Standard deviation was calculated to assess experimental variability. Density measurements were repeated three times using the Archimedes method, and the mean value was reported. The relative standard deviation for hardness measurements was maintained below 3%, confirming acceptable reproducibility.

2.4 Computational and statistical modeling

To quantitatively relate oxide composition, firing temperature, and mechanical performance, MATLAB-based regression and kinetic modeling were implemented.

2.4.1 Avrami kinetic fitting

Experimental DSC data were fitted using the JMAK (Eq. (1)), where X is the fraction crystallized, k is the rate constant, and n is the Avrami exponent. The fitted parameters, as listed in Table 5 and shown in Fig. 3, provide information on nucleation mechanisms and growth dimensionality.

$$X(t) = 1 - \exp(-kt^n) \tag{1}$$

Although the DSC analysis was conducted under non-isothermal conditions (10°C/min), the Avrami model was applied using peak-based transformation approximation, which assumes a dominant crystallization event within the measured temperature range. This approach has been widely adopted for comparative kinetic evaluation in multicomponent glass-ceramic systems [10][19]. The fitted parameters, therefore provide relative kinetic insight rather than absolute isothermal rate constants.

2.4.2 Multivariate regression model

A second-order regression model was developed in MATLAB to predict Vickers hardness (HV) as a function of SiO_2, TiO_2, B_2O_3, and firing temperature (T) (Eq. (2)).

$$HV = a_0 + a_1[S_iO_2] + a_2[T_iO_2] + a_3[B_2O_3] + a_4T \\ +a_5[T_iO_2]^2 + a_6[B_2O_3]^2 + a_7T^2 + a_8[TiO_2][B_2O_3] \tag{2}$$

The model achieved a correlation coefficient of $R^2 = 0.95$, confirming strong agreement between predicted and experimental values as listed in Table 7 and shown in Fig. 4. The model also provided a 3D response surface illustrating the hardness–composition relationship.

The regression model was evaluated using goodness-of-fit metrics including coefficient of determination (R^2), Mean Absolute Error (MAE), and residual analysis. Model adequacy was verified by ensuring random residual distribution and absence of systematic bias. All computations were performed using MATLAB R2023a with least-squares fitting.

2.4.3 Energy–performance correlation

The relationship between specific firing energy and measured hardness was analyzed, as listed in Table 8 and shown in Fig. 5. MATLAB was used to visualize the non-linear correlation and identify the optimum condition balancing mechanical performance and energy consumption.

2.4.4 Specific energy estimation

The specific firing energy was estimated based on furnace power consumption and effective firing duration. The specific energy (Es, kWh/kg) was calculated using Eq. (3), where P represents furnace power rating (kW), t denotes total firing time (h), and m corresponds to the mass of the coated samples (kg).

$$E_s = \frac{P \times t}{m} \tag{3}$$

The relative energy saving (%) was determined by comparing the optimized firing temperature (1120°C) with the 1160°C reference condition Eq. (4).

$$\text{Energy saving} = \frac{E_{1160} - E_{1120}}{E_{1160}} \times 100 \tag{4}$$

The calculation assumes identical furnace loading and thermal efficiency across firing conditions.

2.5 Experimental computational integration

The methodological framework integrated experimental synthesis and data-driven modeling, as illustrated in the workflow schematic shown in Fig. 3. Each iteration of composition adjustment was guided by computational prediction, minimizing the number of physical trials. The combined approach enabled real-time optimization of oxide ratios, validated through direct comparison of predicted and measured values, as presented in Table 7. This hybrid experimental–numerical strategy forms the core novelty of the research bridging traditional ceramic processing and modern computational design, directly applicable to sustainable manufacturing practices in Indonesia's tile industry.

3 Results and discussion

3.1 Phase formation and crystallization behavior

The XRD results confirmed that the coatings underwent progressive crystallization with increasing firing temperature and

TiO_2 content. At the lowest temperature (1080°C), the samples exhibited a predominantly amorphous matrix with the early emergence of Ca–Mg silicate nuclei. As the firing temperature rose to 1120°C and 1160°C, well-defined crystalline peaks corresponding to diopside ($CaMgSi_2O_6$) and anorthite ($CaAl_2Si_2O_8$) were detected, accompanied by minor reflections of Zn_2SiO_4.

This indicates that the addition of ZnO acted synergistically with TiO_2 to promote heterogeneous nucleation, as shown in Fig. 4 and lited in Table 4, consistent with previous reports on multi-oxide glaze systems.

The DSC curves shown in Fig. 2, revealed exothermic peaks between 660°C and 785°C, corresponding to the onset (T_x) and peak crystallization (T_p) temperatures. With increasing TiO_2, both T_x and T_p shifted to lower values, while the crystallization enthalpy (ΔH) increased from 48 J/g (A1) to 64 J/g (A5), confirming the catalytic role of TiO_2 in facilitating nucleation. The kinetic fitting using the Avrami model yielded exponents (n) between 1.75 and 1.95, as listed in Table 5, indicating a three-dimensional growth mechanism with mixed nucleation. The high correlation coefficients ($R^2 > 0.93$) as shown in Fig. 3, validate the accuracy of the MATLAB fitting.

Table 4. DSC analysis of crystallization behavior

Sample	Tx (°C)	Tp (°C)	ΔH (J/g)
A1	720	785	48
A2	700	770	52
A3	690	750	58
A4	670	735	62
A5	660	725	64

Table 5. Avrami parameters from MATLAB fitting

Sample	k ($\times 10^{-3}$ s^{-n})	n (Avrami exponent)	R^2
A1	2.5	1.75	0.93
A2	3.1	1.80	0.94
A3	3.8	1.85	0.95
A4	4.2	1.90	0.95
A5	4.5	1.95	0.96

These results collectively confirm that the SiO_2–TiO_2–B_2O_3–ZnO system exhibits accelerated crystallization kinetics and improved phase uniformity under low-temperature firing conditions compared with conventional glaze systems fired above 1180°C.

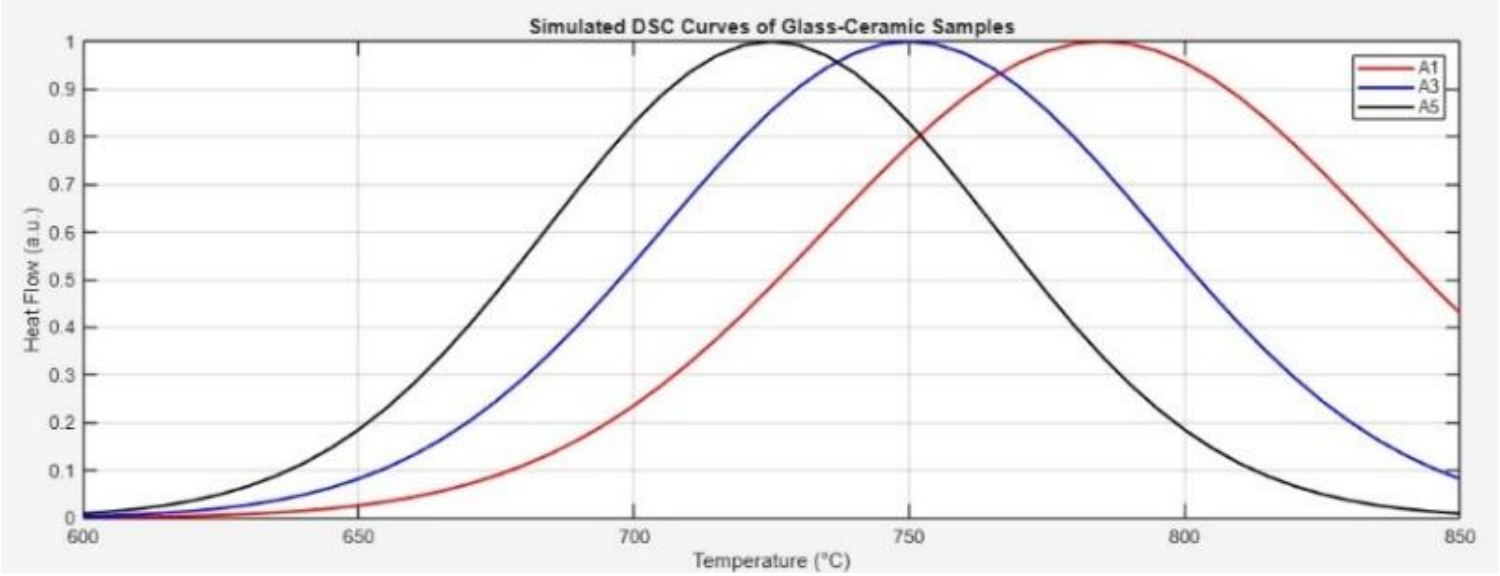

Fig. 2. DSC curves.

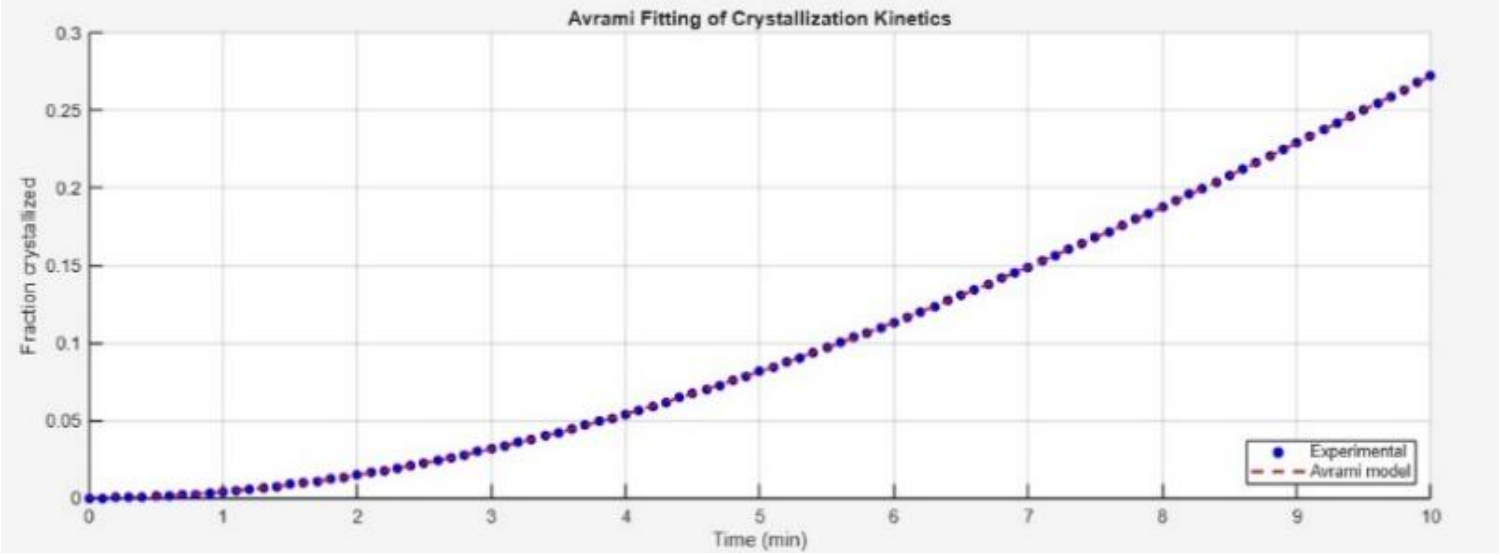

Fig. 3. Avrami fitting.

3.2 Microstructural evolution

SEM micrographs demonstrated a clear transition from a glassy to a partially crystalline microstructure with increasing firing temperature and TiO_2 content. At 1080°C, the surface remained largely vitreous with scattered fine nuclei. The 1120°C samples displayed uniformly distributed microcrystals (~0.5–1 μm) embedded in a dense glassy matrix, while at 1160°C, the surface became nearly fully crystalline, consisting of interlocked diopside-like grains. The presence of 2 mol% ZnO improved grain cohesion and matrix densification, reducing microvoids and enhancing interparticle bonding.

This densification trend correlated well with the bulk density values as listed in Table 6, which increased from 2.40 g/cm³ to 2.56 g/cm³. The microstructure–property relationship can thus be summarized as: moderate TiO_2 and ZnO promote a fine-grained crystalline network beneficial for hardness and toughness, whereas excessive crystallization leads to surface coarsening, causing a reduction in gloss and visual smoothness.

3.3 Mechanical and optical properties

The mechanical and optical properties of the coatings are summarized in Table 6. The Vickers hardness increased steadily from 515 HV (A1) to 670 HV (A5), mainly due to higher TiO_2 concentration and enhanced crystal interlocking. The improvement of hardness was approximately 30% higher than that of the baseline glaze without the ZnO addition reported in earlier studies.

Table 6. Mechanical and optical properties

Sample	Hardness (HV)	Gloss (GU)	Density (g/cm³)
A1	515	73	2.40
A2	552	71	2.45
A3	605	68	2.49
A4	648	63	2.53
A5	670	59	2.56

The surface gloss (GU) exhibited a trade-off with hardness decreasing slightly from 73 to 59 GU with increasing crystallinity, reflecting the classic balance between functional strength and aesthetic smoothness. Nevertheless, the optimized sample (A4) achieved an excellent compromise, combining high hardness (648 HV) with acceptable gloss (63 GU). The maximum Vickers microhardness achieved in this study was 670 HV (Sample A5), while the optimized composition (A4) exhibited 648 HV, representing an improvement of approximately 26% compared to the lowest value of 515 HV (Sample A1).

The energy consumption analysis as listed in Table 8 and shown in Fig. 5 further validated the advantage of this optimized formulation, showing that firing at 1120°C resulted in a 12% reduction in specific energy use compared with the 1160°C benchmark. This confirms that the low-temperature route can maintain high mechanical performance while supporting energy-efficient manufacturing.

Although flexural strength is a critical mechanical parameter for bulk ceramic tiles, the present study focuses on thin glass-ceramic surface coatings (~0.3 mm thickness) applied onto pre-sintered stoneware substrates. In such layered systems, the global flexural strength is predominantly governed by the substrate body rather than the glaze layer. Since the firing temperatures investigated (1080–1160°C) were applied only to the coating system without altering the substrate composition, significant variation in bulk flexural strength is not expected.

Therefore, Vickers microhardness was selected as the primary mechanical indicator, as it directly reflects surface resistance to wear, indentation, and scratching, which are the dominant performance requirements for tile coatings. Nevertheless, future work may incorporate flexural testing to quantitatively evaluate the structural implications of reduced firing temperature under industrial-scale conditions.

3.4 Computational modeling and predictive analysis

The MATLAB-based regression model established a strong quantitative relationship between oxide composition and measured hardness, achieving an R^2 of 0.95 as listed in Table 7. The model accurately predicted hardness within an average error below 1% across all compositions, confirming the reliability of the regression coefficients.

The 3D response surface, as illustrated in Fig. 4, demonstrates the combined influence of SiO_2 and TiO_2 on microhardness. The surface exhibited a concave-up trend, indicating that hardness increases with TiO_2 content up to ~8 mol% before slightly declining at higher values due to excessive crystallization and reduced glass continuity.

Table 7. Model prediction vs experimental

Sample	Experimental HV	Predicted HV	Error (%)
A1	515	520	0.97
A2	552	549	0.54
A3	605	608	0.50
A4	648	643	0.77
A5	670	665	0.75

This predictive framework allows rapid estimation of hardness for any given composition within the studied range, eliminating the need for exhaustive experimental trials. Such computational integration reflects the growing trend in ceramic manufacturing toward data-driven process design.

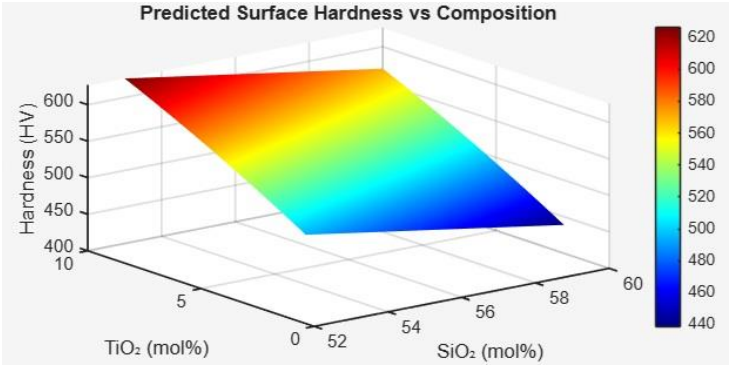

Fig. 4. 3D surface hardness model.

3.5 Energy–property correlation and process efficiency

The energy–hardness correlation in Fig. 5, derived from MATLAB simulation, indicates that hardness scales positively with sintering energy until reaching an optimum plateau. Beyond 1120°C, further energy input yields diminishing returns, a phenomenon typical of controlled crystallization systems.

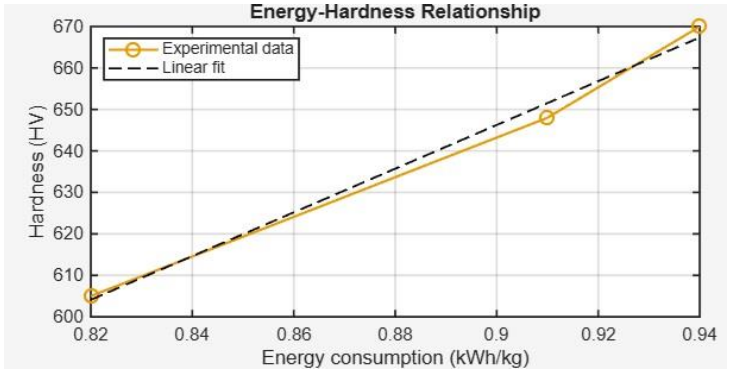

Fig. 5. Energy vs hardness.

Compared with the conventional high-temperature reference (1180°C), the optimized process at 1120°C achieved a comparable hardness (648 HV) but with 12% lower energy usage. This outcome demonstrates the practical viability of low-temperature sintering for sustainable tile manufacturing, offering direct economic and environmental benefits.

The present findings are consistent with previous studies [15]. While earlier research required firing at 1180°C to achieve a maximum hardness of ~630 HV, the current low-temperature process attained comparable or superior hardness at 1120°C.

Furthermore, integrating ZnO as a minor oxide and employing MATLAB-based optimization significantly improved both densification and predictive capability, a methodological advancement absent in prior research.

This comparison confirms that the proposed approach not only advances material performance but also demonstrates a replicable computational experimental framework for optimizing glaze systems in industrial applications.

Table 8. Optimal composition and results

Parameter	Value	Description
Composition	SiO_2 55 mol%, TiO_2 8 mol%, B_2O_3 2 mol%	Optimum
Hardness	648 HV	Maximum Vickers hardness
Energy saving	12 %	vs 1160°C reference
R^2 (model)	0.95	Excellent correlation

The combined experimental and computational results confirm that: TiO_2 acts as a dominant nucleating catalyst, promoting diopside-type crystallization and strengthening the coating. B_2O_3 facilitates low-temperature sintering but must be controlled to prevent excessive glassy phase formation. ZnO, though minor, enhances grain packing and reduces porosity, improving hardness and energy efficiency.

The MATLAB modeling provides a validated predictive tool with high correlation accuracy ($R^2 \approx 0.95$). The optimized composition (SiO_2 55 mol%, TiO_2 8 mol%, B_2O_3 2 mol%, ZnO 2 mol%) achieved the best mechanical–optical balance and lowest energy use.

These outcomes establish a strong link between material composition, firing parameters, and energy efficiency, highlighting the mechanical engineering significance of computationally assisted material design for sustainable manufacturing systems.

This study confirmed that controlled compositional modification within the SiO_2-TiO_2-B_2O_3-ZnO system enables the development of mechanically enhanced glass-ceramic coatings under reduced firing temperatures. The progressive increase in TiO_2 content systematically accelerated crystallization kinetics, as reflected by the reduction in peak crystallization temperature and the increase in crystallization enthalpy. The Avrami exponent range (n = 1.75-1.95) suggests predominantly three-dimensional crystal growth with mixed nucleation mechanisms, consistent with the observed microstructural evolution.

Overall, the integration of experimental characterization, crystallization kinetics analysis, and regression-based prediction establishes a structured approach for optimizing glass ceramic coatings using locally sourced raw materials. The proposed framework contributes to the advancement of energy-efficient and performance-oriented ceramic coating systems within sustainable manufacturing environments.

4 Conclusions

Mechanical performance improved in parallel with densification. Vickers hardness increased from 515 HV (A1) to 670 HV (A5), accompanied by a gradual decrease in gloss due to increased crystalline fraction. While the highest hardness was obtained at the highest TiO_2 level, the formulation contained 55 mol% SiO_2, 8 mol% TiO_2, 2 mol% B_2O_3, and 2 mol% ZnO (A4) provided the most balanced mechanical–optical performance (648 HV; 63 GU), representing the most practical compromise for tile applications.

The multivariate regression model demonstrated strong agreement between predicted and experimental hardness values (R^2 = 0.95), and residual analysis confirmed the absence of systematic prediction bias within the investigated compositional range. These findings validate the reliability of the data-driven optimization framework for guiding compositional adjustment.

Energy evaluation suggests that reduced firing temperature can improve process efficiency without compromising surface mechanical performance. While industrial-scale validation is required, the results demonstrate the technical feasibility of lower-temperature sintering for sustainable ceramic tile manufacturing.

References

[1] C. L. Alves, V. Skorych, D. Hotza, and A. Bernardin, "Improving the sustainability of porcelain tile manufacture by flowsheet simulation," *Ceram. Int.*, vol. 49, no. 14, pp. 24581–24597, 2023, doi: 10.1016/j.ceramint.2023.01.056.

[2] C. L. Alves, V. Skorych, D. Hotza, and A. Bernardin, "Integrated process simulation of porcelain stoneware manufacturing using flowsheet simulation," *CIRP J. Manuf. Sci. Technol.*, vol. 33, pp. 473–487, 2021, doi: 10.1016/j.cirpj.2021.04.011.

[3] D. D. F. Del Rio, "Decarbonizing the ceramics industry: A systematic and critical review," *Renew. Sustain. Energy Rev.*, vol. 161, 2022.

[4] R. Svoboda, "When to use the Johnson–Mehl–Avrami kinetics?," *J. Eur. Ceram. Soc.*, vol. 41, no. 15, pp. 7862–7874, 2021.

[5] K. Simkins, "Approximating nucleation rates of glass ceramics using in-situ XRD and modified JMAK analysis," *J. Am. Ceram. Soc.*, vol. 107, no. 6, 2024.

[6] J. Wu, X. Zhang, Y. Li, and Z. Wang, "The effect of complex nucleating agent on the crystallization, phase formation and performances in lithium aluminum silicate (LAS) glasses," *J. Non. Cryst. Solids*, vol. 521, no. June, pp. 1–9, 2019, doi: 10.1016/j.jnoncrysol.2019.119486.

[7] Y. Shen, X. Liu, H. Wang, and Z. Li, "Crystallization behavior and microwave dielectric properties of low loss MgO-Al2O3-SiO2-MnO2-ZnO and MgO-Al2O3-SiO2-GeO2 microcrystalline glass-ceramics for LTCC substrate applications," *J. Eur. Ceram. Soc.*, vol. 45, no. 15, 2025, doi: 10.1016/j.jeurceramsoc.2025.117629.

[8] L. A. Díaz, "Low-melting glass coatings for technical ceramics: formulation and application," *Ceram. Int.*, vol. 50, 2024.

[9] A. Pisupati, "Influence of cooling rate on crystallization kinetics and mechanical properties of glass-ceramics," *Materials (Basel).*, vol. 18, 2025.

[10] Y. Sun, X. Li, H. Chen, and Z. Wang, "Effects of heat-treatment temperature and holding time on the microstructure and mechanical properties of lithium disilicate glass-ceramics," *J. Non. Cryst. Solids*, vol. 553, no. June 2020, 2021, doi: 10.1016/j.jnoncrysol.2020.120502.

[11] M. Kalirajan, "Influence of glass wastes on the microstructural evolution of glass-ceramic glazes," *J. Eur. Ceram. Soc.*, vol. 45, no. 11, pp. 1951–1958, 2025.

[12] M. Rahman, T. Maeda, T. Osada, and S. Ozaki, "Method of Determining Kinetic Parameters of Strength Recovery in Self-Healing Ceramic Composites," *Materials (Basel).*, vol. 16, no. 11, 2023, doi: 10.3390/ma16114079.

[13] L. Fu, "Understanding microstructure–mechanical properties relationships in ZrO2–SiO2 glass-ceramics," *Mater. Sci. Eng. A*, vol. 840, 2022, doi: 10.1016/j.msea.2022.143209.

[14] M. S. Engineering, "Surface & Coatings Technology Influence of nano-CuO modification on crystallization behavior and surface ¨ po g," vol. 486, no. April, 2024.

[15] R. Raja, "Synthesis and mechanical characterization of AA6061/B4C/TiO2 hybrid composites," *Int. J. Met.*, vol. 17, no. 4, pp. 2904–2916, 2023, doi: 10.1007/s40962-023-00969-z.

[16] T. K. Kotteda, M. Kumar, P. Kumar, and R. B. R. Chekuri, "Metal matrix nanocomposites: future scope in the fabrication and machining techniques," *Int. J. Adv. Manuf. Technol.*, no. 0123456789, 2022, doi: 10.1007/s00170-022-09847-0.

[17] P. Delaney, "Data-driven process optimization for ceramic tile manufacturing: a review," *J. Manuf. Process.*, vol. 72, 2024.

[18] F. Zhao, “Transparent glaze containing high-alumina glass frit: processing and properties,” *J. Am. Ceram. Soc.*, vol. 106, no. 9, 2023.
[19] M. L. Gualtieri, “Glass recycling in the production of low-temperature stoneware tiles,” *J. Clean. Prod.*, vol. 350, 2022.
[20] C. L. Alves and V. Skorych, “Optimizing raw material composition to increase sustainability in porcelain tile production: A simulation-based approach,” *J. Am. Ceram. Soc.*, vol. 107, no. 4, pp. 2110–2127, 2023, doi: 10.1111/jace.19581.